Cancer Therapy: Preclinical

Clinical Cancer Research

Targeting the PI3K Pathway in the Brain—Efficacy of a PI3K Inhibitor Optimized to Cross the Blood–Brain Barrier

Laurent Salphati[1], Timothy P. Heffron[2], Bruno Alicke[3], Merry Nishimura[3], Kai Barck[4], Richard A. Carano[4], Jonathan Cheong[1], Kyle A. Edgar[3], Joan Greve[4], Samir Kharbanda[3], Hartmut Koeppen[5], Shari Lau[5], Leslie B. Lee[3], Jodie Pang[1], Emile G. Plise[1], Jenny L. Pokorny[6], Hani Bou Reslan[4], Jann N. Sarkaria[6], Jeffrey J. Wallin[3], Xiaolin Zhang[1], Stephen E. Gould[3], Alan G. Olivero[2], and Heidi S. Phillips[3]

Abstract

Purpose: Glioblastoma (GBM), the most common primary brain tumor in adults, presents a high frequency of alteration in the PI3K pathway. Our objectives were to identify a dual PI3K/mTOR inhibitor optimized to cross the blood–brain barrier (BBB) and characterize its brain penetration, pathway modulation in the brain and efficacy in orthotopic xenograft models of GBM.

Experimental Design: Physicochemical properties of PI3K inhibitors were optimized using in silico tools, leading to the identification of GNE-317. This compound was tested in cells overexpressing P-glycoprotein (P-gp) or breast cancer resistance protein (BCRP). Following administration to mice, GNE-317 plasma and brain concentrations were determined, and phosphorylated biomarkers (pAkt, p4EBP1, and pS6) were measured to assess PI3K pathway suppression in the brain. GNE-317 efficacy was evaluated in the U87, GS2, and GBM10 orthotopic models of GBM.

Results: GNE-317 was identified as having physicochemical properties predictive of low efflux by P-gp and BCRP. Studies in transfected MDCK cells showed that GNE-317 was not a substrate of either transporter. GNE-317 markedly inhibited the PI3K pathway in mouse brain, causing 40% to 90% suppression of the pAkt and pS6 signals up to 6-hour postdose. GNE-317 was efficacious in the U87, GS2, and GBM10 orthotopic models, achieving tumor growth inhibition of 90% and 50%, and survival benefit, respectively.

Conclusions: These results indicated that specific optimization of PI3K inhibitors to cross the BBB led to potent suppression of the PI3K pathway in healthy brain. The efficacy of GNE-317 in 3 intracranial models of GBM suggested that this compound could be effective in the treatment of GBM. *Clin Cancer Res; 18(22); 6239–48. ©2012 AACR.*

Introduction

The phosphatidylinositol 3-kinase (PI3K) pathway plays a key role in cell survival, growth and proliferation (1). The lipid kinases belonging to the PI3K family phosphorylate the 3′-hydroxyl group of phophatidylinositols, which lead to the activation of the serine/threonine protein kinase Akt. Further downstream effectors include the mTOR complex 1 and S6 kinase. From the 3 classes of PI3K, class Ia is the most widely involved in cancer and its kinases are composed of a catalytic (p110α, p110β, or p110δ) and a regulatory subunit (p85 or p55). The phophatase PTEN acts as a tumor suppressor and inhibits PI3K pathway signaling (2).

PI3K deregulation, through activating mutations of the p110α catalytic subunit or suppression of PTEN, has been associated with the development of numerous cancers (3). More specifically, alteration of this pathway has been detected in more than 80% of glioblastoma (GBM; refs. 4, 5). GBM is the most common and aggressive primary tumor of the central nervous system (CNS) in adults. This high grade glioma, characterized by rapid growth and diffuse invasiveness (6), presents very few treatment options. Tumor progression is controlled only for a limited time with a median survival duration of less than 2 years after initial diagnosis (7). Key signaling proteins of the PI3K pathway are mutated in a large proportion of GBM, leading to persistent activation of the pathway; EGFR amplification and/or mutation, mutation of the PI3K catalytic and regulatory subunits, and loss of PTEN protein are detected in 45%, 10%, and 50% of GBM, respectively (4). Thus, targeting the PI3K pathway represents an attractive therapeutic approach for brain tumors. Inhibitors of mTOR, a key mediator of PI3K signaling, have been evaluated in Phase

Authors' Affiliations: Departments of [1]Drug Metabolism and Pharmacokinetics, [2]Chemistry, [3]Cancer Signaling and Translational Oncology, [4]Biomedical Imaging, [5]Pathology, Genentech Inc, South San Francisco, California; and [6]Mayo Clinic, Department of Radiation Oncology, Rochester, Minnesota

Note: Supplementary data for this article are available at Clinical Cancer Research Online (http://clincancerres.aacrjournals.org/).

Corresponding Author: Laurent Salphati, Department of Drug Metabolism and Pharmacokinetics, Genentech, Inc., 1 DNA Way, South San Francisco, CA 94080. Phone: 650-467-1796; Fax: 650-467-3487; E-mail: salphati.laurent@gene.com

doi: 10.1158/1078-0432.CCR-12-0720

Translational Relevance

Activation of the PI3K pathway, through mutations of its components, is observed in more than 80% of glioblastoma (GBM), the most common and aggressive type of malignant primary brain tumor. This pathway can also be activated by therapeutic interventions, such as radiation and chemotherapy. Thus, inhibition of the PI3K pathway represents an attractive therapeutic approach for GBM. However, the diffusely infiltrative nature of GBM requires the pharmacologic agents to cross the blood–brain barrier (BBB). Here we show that GNE-317, a PI3K/mTOR inhibitor that was specifically designed to cross the BBB, achieved potent suppression of the PI3K pathway in the brain of mice with intact BBB. GNE-317 was also efficacious in 3 orthotopic models of GBM, U87, GS2, and GBM10. These results suggest that PI3K suppression and GBM tumor growth inhibition may be achieved in patients, including in areas with intact BBB, provided that efficient brain and tumor penetration is obtained.

I and II clinical trials as single agents or in combination with receptor tyrosine kinase inhibitors with limited success (4). These compounds, analogues of rapamycin, mostly target mTORC1. This in turn can trigger a feedback loop, possibly through mTORC2, which results in the activation of Akt (6, 8). Recent work from Tanaka and colleagues also points to a role of mTORC2 signaling, independent of mTORC1, in GBM (9). The disappointing results with rapalogues may also be attributed to the failure of the drugs to fully access their target (4). These 2 points underscore the potential improvement in activity that could be achieved with dual PI3K/mTOR inhibitors (mTORC1 and mTORC2) as well as the challenge in crossing the BBB and overcoming the protective effect of efflux transporters to reach the brain and tumors with anticancer agents.

The objectives of the studies presented here were to identify a potent dual PI3K/mTOR inhibitor possessing physicochemical properties specifically optimized for brain penetration, and test whether this compound, GNE-317 (Fig. 1A), could show PI3K pathway suppression in the brain and superior efficacy in intracranial models of GBM.

Materials and Methods

Chemicals

All GNE compounds, including GNE-317, GDC-0941, and GDC-0980, were synthesized by Genentech, Inc. All solvents used in analytic assays were purchased from Thermo Fisher Scientific and were of analytic or high-performance liquid chromatography grade. All other chemicals and reagents were purchased from Sigma-Aldrich unless specified.

Determination of physicochemical properties and Central Nervous System Multiparameter Optimization (CNS-MPO) score

Using MoKa Software (version 1.1.0, Molecular Discovery) and a custom pKa model augmented with Roche internal data, logarithm of the acid dissociation constant of most basic center (cpK_{a_MB}), logarithm of the partition

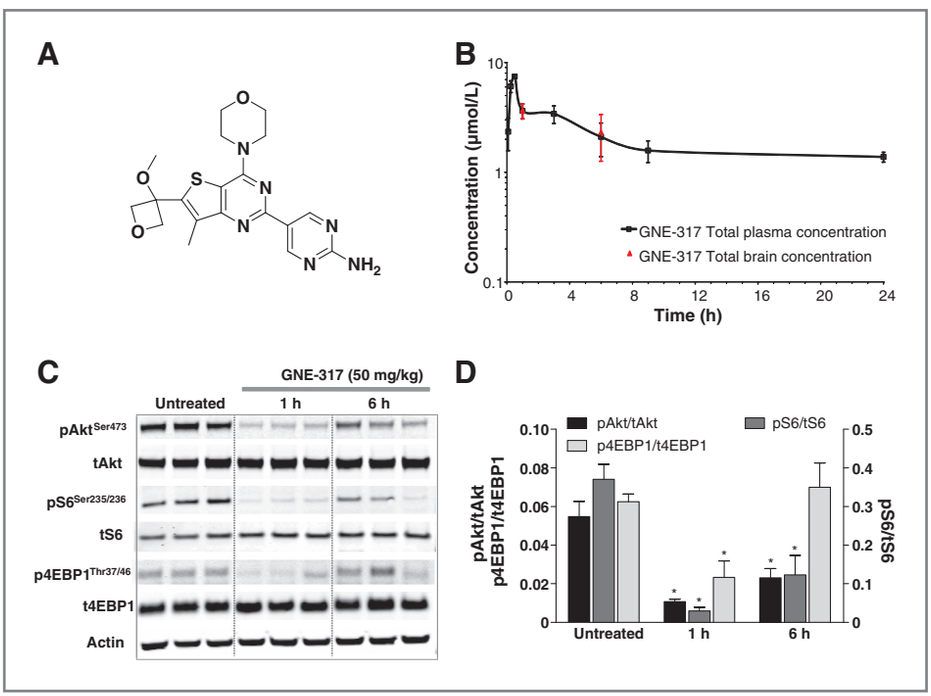

Figure 1. A, chemical structure of GNE-317. B, plasma concentration-time profile and brain concentrations of GNE-317 following PO administration (50 mg/kg) to CD-1 mice. C, Western blotting of mouse brains probed with antibodies against pAkt, total Akt, pS6, total S6, p4EBP1, total 4EBP1 and actin. D, quantitation of pAkt/total Akt, p4EBP1/total 4EBP1 and pS6/total S6 at 1 and 6 hours postdose in CD-1 mice. B and D, results are presented as the mean ± S.E. of 3 animals. *, significantly different from control. $P < 0.05$, *t*-test.

coefficient (clogP), and logarithm of the distribution coefficient at pH 7.4 (clogD) were calculated. Using OEChem tools (OpenEye Scientific Software), molecular mass (MM), topologic polar surface area (TPSA), number of hydrogen bond donors (HBD) were computed for molecules in their neutral form. CNS-MPO scores were calculated using the formula proposed by Wager and colleagues (10). To verify our implementation of CNS-MPO, we compared our scores with the published data set and found an excellent correlation.

In vitro transport assays

Madin-Darby canine kidney (MDCK) cells heterologously expressing human P-gp, human BCRP or mouse Bcrp1 and LLC-PK1 cells transfected with mouse P-gp (mdr1a) were used to determine whether GNE-317 was a substrate of these transporters. MDR1-MDCKI cells were licensed from the National Cancer Institute whereas Bcrp1-MDCKII, BCRP-MDCKII, and Mdr1a-LLC-PK1 cells were obtained from the Netherlands Cancer Institute. For transport studies, cells were seeded on 24-well Millicell plates (Millipore) 4 days before use (polyethylene terephtalate membrane, 1 μmol/L pore size) at a seeding density of 2.5×10^5 cells/mL (except for MDR1-MDCKI, 1.3×10^5 cells/mL). GNE-317 was tested at 5 μmol/L in the apical to basolateral (A-B) and basolateral to apical (B-A) directions. The compound was dissolved in transport buffer consisting of Hank's balanced salt solution (HBSS) with 10 mmol/L HEPES (Invitrogen Corporation). Lucifer Yellow (Sigma-Aldrich) was used as the paracellular marker. GNE-317 concentrations in the donor and receiving compartments were determined by liquid chromatography/tandem mass spectrometry (LC-MS/MS) analysis. The apparent permeability (P_{app}), in the A-B and B-A directions, was calculated after a 2-hour incubation as:$Papp = (dQ/dt)(1/AC0)$,where dQ/dt is the rate of compound appearance in the receiver compartment; A is the surface area of the insert; and C_0 is the initial substrate concentration at T_0.

The efflux ratio (ER) was calculated as ($P_{app,\ B\text{-}A}/P_{app,\ A\text{-}B}$).

Determination of plasma protein and brain binding

The extent of protein binding of GNE-317 was determined *in vitro*, in mouse plasma (Bioreclamation, Inc.) by equilibrium dialysis using a HTDialysis 96-well block (HTDialysis LLC). GNE-317 was added to pooled plasma ($n \geq 3$) at a total concentration of 10 μmol/L. Plasma samples were equilibrated with phosphate-buffered saline (pH 7.4) at 37°C in 90% humidity and 5% CO_2 for 4 hours. Following dialysis, concentration of GNE-317 in plasma and buffer was measured by LC-MS/MS. The percentage GNE-317 unbound in plasma was determined by dividing the concentration measured in the postdialysis buffer by that measured in the postdialysis plasma and multiplying by 100. Incubations were carried out in triplicate. Parameters are presented as mean ± standard deviation (SD).

The free fraction of GNE-317 in mouse brain was determined as described by Kalvass and colleagues (11). In brief, brain tissue was homogenized in 3 volumes of phosphate-buffered saline and GNE-317 was added at a final concentration of 10 μmol/L. Aliquots of 300 μL were dialyzed in a RED device (Thermo Scientific) against a volume of 500 μL buffer for 4 hours at 37°C in an incubator at 90% humidity and 5% CO_2. Following dialysis, tissues, and buffer samples were analyzed as described for the plasma protein binding studies.

In vivo studies

All studies conducted were approved by the Institutional Animal Care and Use Committee at Genentech, Inc. or the Mayo Institutional Animal Care and Use Committee.

Pharmacokinetic study in mouse

Twelve female CD-1 mice (Charles River Laboratories) were given a 50 mg/kg oral (PO) dose of GNE-317 in 0.5% methylcellulose/0.2% Tween 80 (MCT). Two blood samples of approximately 0.15 mL were collected from each mouse ($n = 3$ mice per timepoint) by retro-orbital bleed or terminal cardiac puncture whereas the animals were anesthetized with isoflurane. Blood samples were collected in tubes containing K_2EDTA as the anticoagulant, predose and at 0.083, 0.25, 0.5, 1, 3, 6, 9, and 24 hours postdose. Samples were centrifuged within 1 hour of collection and plasma was collected and stored at −80°C until analysis. Total concentrations of GNE-317 were determined by LC-MS/MS, following plasma protein precipitation with acetonitrile, and injection of the supernatant onto the column, a Varian MetaSil AQ C18 column (50 mm × 2 mm, 5 μm particle size). A CTC HTS PAL autosampler (LEAP Technologies) linked to a Shimadzu SCL-10A controller with LC-10AD pumps (Shimadzu), coupled with an AB Sciex API 4000 triple quadrupole mass spectrometer (AB Sciex) were used for the LC-MS/MS assay. The aqueous mobile phase was water with 0.1% formic acid and the organic mobile phase was acetonitrile with 0.1% formic acid. The lower and upper limits of quantitation of the assay were 0.005 and 10 μmol/L, respectively. The total run time was 1.5 minutes and the ionization was conducted in the positive ion mode. Brains were collected at 1 and 6 hours postdose from 3 different animals at each time point, rinsed with ice-cold saline, weighed and stored at −80°C until analysis. For GNE-317 quantitation, mouse brains were homogenized in 3 volumes of water. The homogenates were extracted by protein precipitation with acetonitrile. LC-MS/MS analysis was conducted as described for the plasma. Brain homogenate concentrations were converted to brain concentrations for the calculations of brain-to-plasma ratios.

Modulation of pAKT, p4EBP1, and pS6 in brain

Female CD-1 mice were administered a single PO dose of GNE-317 at 50 mg/kg. Brains and plasma were collected at 1 and 6 hour postdose, from 3 animals at each time point. Individual brains were split in half for PD analysis and GNE-317 concentration measurement. The samples were stored at −70°C and analyzed for GNE-317 total concentration as described previously. For PD analysis, cell

extraction buffer (Invitrogen) containing 10 mmol/L Tris pH 7.4, 100 mmol/L NaCl, 1 mmol/L EDTA, 1 mmol/L EGTA, 1 mmol/L NaF, 20 mmol/L $Na_4P_2O_7$, 2 mmol/L Na_3VO_4, 1% Triton X-100, 10% glycerol, 0.1% SDS, and 0.5% deoxycholate was supplemented with phosphatase, protease inhibitors (Sigma) and 1 mmol/L PMSF and added to frozen brain biopsies. Brains were homogenized with a small pestle (Konte Glass Company), sonicated briefly on ice, and centrifuged at 20,000 × *g* for 20 minutes at 4°C. Protein concentration was determined using BCA protein assay (Pierce). Proteins were separated by electrophoresis and transferred to NuPage nitrocellulose membranes (Invitrogen). Licor Odyssey Infrared detection system (Licor) was used to assess and quantify protein expression. PI3K/mTOR pathway markers were evaluated by immunoblotting using antibodies against $pAkt^{Ser473}$, total Akt, $p4EBP1^{Thr37/46}$, total 4EBP1, $pS6^{Ser235/236}$, and total S6 (Cell Signaling). The differences in marker levels between the treated and control mice were evaluated using the Student *t* test (Excel v14.0, Microsoft).

Efficacy studies in brain tumor models

Three human glioma models were used in the *in vivo* studies: The U-87 MG/M (U87) glioblastoma cancer cells (a Genentech variant of U-87 MG cells from American Type Culture Collection), the GS 2.Luc cells (GS2) derived from GS 2 glioblastoma cells (12) and the *in vivo*-passaged GBM10 model (13). These 3 models are PTEN-deficient, with the GS2 cell line presenting a copy number loss at the PTEN locus (12), and no detectable PTEN protein by western blot (14). The identity of the U87 and GS2 lines was confirmed by STR profiling (DNA Diagnostics Center). Cells used for *in vivo* studies were harvested within 5 passages of the material used to confirm authenticity. The U87 (250K), GS2 (100K), and GBM10 (300K) tumor cells were injected via stereotaxic surgery into the right striatum in a volume of 3 to 5 μL. For each experiment, mice were randomized into groups of 10 to obtain comparable mean tumor volumes between treatment and control groups for each model. In addition, U87 tumors could be monitored by bioluminescence, which confirmed mean tumor volumes were similar across groups (Supplementary Table 1). Although the randomization of animals into groups to obtain comparable mean tumor volumes before treatment was an appropriate approach in our studies, baseline imaging (before treatment) would obviously be necessary and collected during a clinical trial. Treatments were initiated at a time that ensured that the blood–brain barrier (BBB) had recovered from surgical disruption and tumors were expanding. Previous studies conducted in our laboratories in intracranial models (and including sham surgery) indicated that the BBB had recovered from the disruption caused by the surgery after 7 days. Mice bearing intracranial U87 xenografts were administered GNE-317 (40 mg/kg), GDC-0941 (250 mg/kg), or vehicle (0.5% methylcellulose/0.2%Tween 80; MCT) PO daily for 3 weeks starting 7 days posttumor cell inoculation. Mice bearing intracranial GS2 xenografts were administered GNE-317 (40 mg/kg), GDC-0941 (250 mg/kg), GDC-0980 (10 mg/kg), or vehicle (MCT) PO daily for 6 weeks starting 14 days posttumor cell inoculation. Mouse body weights were recorded twice per week during the study and animals were euthanized if body weight loss was greater than 20% from their initial body weight. Mice bearing intracranial xenografts from GBM10 were treated with the vehicle alone or GNE-317. GNE-317 was administered PO daily, initially at a dose of 40 mg/kg/day for 2 weeks and then subsequently at 30 mg/kg/day. All GBM10 tumor-bearing mice were observed daily and euthanized upon reaching a moribund state. Tumor volumes were monitored by *ex vivo* micro-CT and T2 MRI for the GBM models U87 and GS2, respectively. The differences between treatment groups were evaluated using the Dunnett's *t* test in JMP (SAS Institute). MRI was carried out on a Varian 9.4T MRI system with a 30 mm quadrature volume coil. During the imaging, animals were kept under anesthesia with 2% isoflurane in air. Body temperature was continuously monitored using a rectal probe and was maintained at 37°C by a heated-air flow system regulated by in-house LabVIEW controller software. A T2-weighted fast spin echo, multi-slice (FSEMS) sequence was used to detect lesions by MRI. Twelve to twenty axial 0.5 to 0.8-mm-thick slices were acquired with a 20 mm × 20 mm field of view (FOV), and 128 × 128 matrix, zero-filled to 256 × 256 images. TR = 3,500 to 4,000 ms, TE = 9 to 10 ms, ETL = 8, k-zero = 4, NEX = 8.The BBB integrity was evaluated by dynamic contrast enhanced MRI (DCE-MRI). Precontrast 3D gradient echo (3DGE) datasets were acquired at 2° and 10° flip angles, TR = 8.3 ms, TE = 1.1 ms, NEX = 4, FOV = 20 × 20 × 8 mm, matrix = 64 × 64 × 16. A 50 μL bolus injection of Gd-based Gadodiamide (Omniscan) contrast agent was injected via a tail vein catheter following collection of the precontrast images. Postcontrast 3DGE images were then acquired approximately every 10 seconds for 30 minutes (10° flip angle, NEX = 1). Tumor volumes were calculated from the T2-weighted FSEMS images using an intensity threshold based region growing tool in MRVision software. Sample preparation, scanning, and image analysis for ex-vivo micro-computed tomography (micro-CT) imaging were carried out as described previously (15). In the studies conducted with the GS2 tumor-bearing mice, plasma and brains were also collected at the end of treatment to measure the concentration of each compound. Each brain was bissected into a normal and tumor-bearing hemisphere. Plasma and brains were processed and analyzed by LC-MS/MS as described previously.

Modulation of the PI3K pathway in intracranial tumors

The effects of GNE-317 and GDC-0941 on the PI3K pathway in GS2 and U87 orthotopic tumors were evaluated by immunohistochemistry (IHC) following a single PO dose of GDC-0941 (250 mg/kg) or GNE-317 (40 mg/kg) to mice. Brains were collected 1 hour postdose, after the animals had been anesthetized with pentobarbital, perfused first with heparinized phosphate-buffered saline and subsequently with 4% paraformaldehyde.

IHC for detection of pAKT with antibody D9E (Cell Signaling Technologies) was carried out on 4-μ-thick paraffin-embedded tissue sections using a Discovery XT autostainer and CC1 standard antigen retrieval (Ventana Medical Systems). Specifically bound primary antibody was detected using OmniMap detection (Ventana) and hematoxylin counterstain.

Results

Optimization of physicochemical properties

Calculated physicochemical parameters (cLogP, cLogD, cpKa, MM, TPSA, and HBD) were used to determine the Central Nervous System Multiparameter Optimization (CNS-MPO) score. Higher ERs in MDCK cells transfected with P-gp (Supplementary Fig. 1A) or bcrp1 (Supplementary Fig. 1B) were associated with lower values of the CNS-MPO score. In addition, most compounds with ER lower than 3 (cut-off value for our assay) also appeared to present CNS-MPO scores greater than 4.5; 16 of 21 compounds in the P-gp assay, and 22 of 23 compounds in the bcrp1 assay. In contrast, the majority of the compounds with ER greater than 3 had a CNS-MPO score lower than 4.5 in both assays.

Transport studies in transfected cell lines

The bidirectional transport of GNE-317 was assessed in transfected cell lines overexpressing human or mouse P-gp or BCRP. The apparent permeability (P_{app}) was high and comparable to that determined for metoprolol, the high P_{app} marker used in the same experiments (data not shown). The ERs ($P_{app,\ B\text{-}A}/P_{app,\ A\text{-}B}$) were not markedly different from 1 in the MDCK or LLC-PK1 transfected cells (Table 1), indicating that GNE-317 was not impacted by the overexpression of the human or mouse P-gp and BCRP, and suggesting that this compound was a poor substrate of these transporters.

Table 1. Apparent permeability (P_{app}) of GNE-317 in transfected cells

	P_{app} (10^{-6} cm/s)		P_{app} ratio
Cell line	A to B	B to A	B-A/A-B
MDR1-MDCKI	9.84 ± 0.66	15.1 ± 1.62	1.54 ± 0.26
Bcrp1-MDCKII	16.2 ± 1.91	15.1 ± 2.48	0.95 ± 0.28
BCRP-MDCKII	14.2 ± 1.13	16.0 ± 1.60	1.13 ± 0.14
Mdr1a-LLC-PK	13.1 ± 0.61	15.7 ± 0.50	1.20 ± 0.09

Results reported as mean ± S.D. ($n = 3$).

Plasma protein and brain tissues binding

Binding of GNE-317 to plasma proteins was moderate, with a free fraction (%) of 14.9 ± 1.6 ($n = 3$) in mouse plasma, when tested at 10 μmol/L. Binding to brain tissues was higher, with a free fraction of 5.4% (± 0.5; $n = 3$).

Pharmacokinetics of GNE-317 in mouse

The plasma concentrations-time profile of GNE-317 following a single PO administration (50 mg/kg) to mice is presented in Fig. 1B. Plasma concentrations remained fairly constant and higher than 2 μmol/L up to 9 hours postdose. GNE-317 free brain concentrations between 1 and 6 hours were higher than 0.1 μmol/L, suggesting that GNE-317 would be able to modulate the PI3K pathway in the brain. The brain-to-plasma ratio of total concentrations remained unchanged and was approximately 1 between 1 and 6 hours postdose (Table 2). Free brain-to-free plasma concentrations ratio was 0.3.

Modulation of pAkt, p4EBP1, and pS6 in brain

The levels of pAkt, p4EBP1, and pS6 (downstream markers of the PI3K/mTOR pathway) measured in the brain of normal mice that received a single oral dose of GNE-317 (50 mg/kg) were significantly lower than those in the control animals (Fig. 1C), with suppression of pAkt, p4EBP1, and pS6 reaching 80%, 84%, and 92%, respectively, 1 hour postdose and remaining greater than 55% 6 hours postdose for pAkt and pS6 (Fig. 1D). Levels of p4EBP1 were back to baseline 6 hours postdose.

Efficacy in brain tumor models

The efficacy of GNE-317 was tested in 3 intracranial tumor models, the U87, the neurosphere GS2 and the GBM10 models. GNE-317 was administered PO at 40 mg/kg daily for 3 and 6 weeks to U87 and GS2 tumor-bearing mice, respectively, and for more than 12 weeks to GBM10 tumor-bearing mice. The effect of the treatment on the U87 and GS2 tumor volumes was assessed at the end of the dosing period. A U87 tumor image obtained by micro-CT is presented in Fig. 2C. GNE-317 reduced the U87 tumor volumes by more than

Table 2. Plasma concentrations, brain concentrations and brain-to-plasma ratio of GNE-317 following PO administration (50 mg/kg) to mice

Time	Total			Free		
postdose (hours)	Brain (μmol/L)	Plasma (μmol/L)	Brain-to-plasma ratio	Brain (μmol/L)	Plasma (μmol/L)	Brain-to-plasma ratio
1	3.64 ± 0.95	3.63 ± 0.98	1.01 ± 0.05	0.19 ± 0.05	0.58 ± 0.15	0.33 ± 0.01
6	2.31 ± 1.82	2.10 ± 1.23	1.00 ± 0.27	0.12 ± 0.09	0.34 ± 0.19	0.33 ± 0.09

Results reported as mean ± S.D. ($n = 3$).

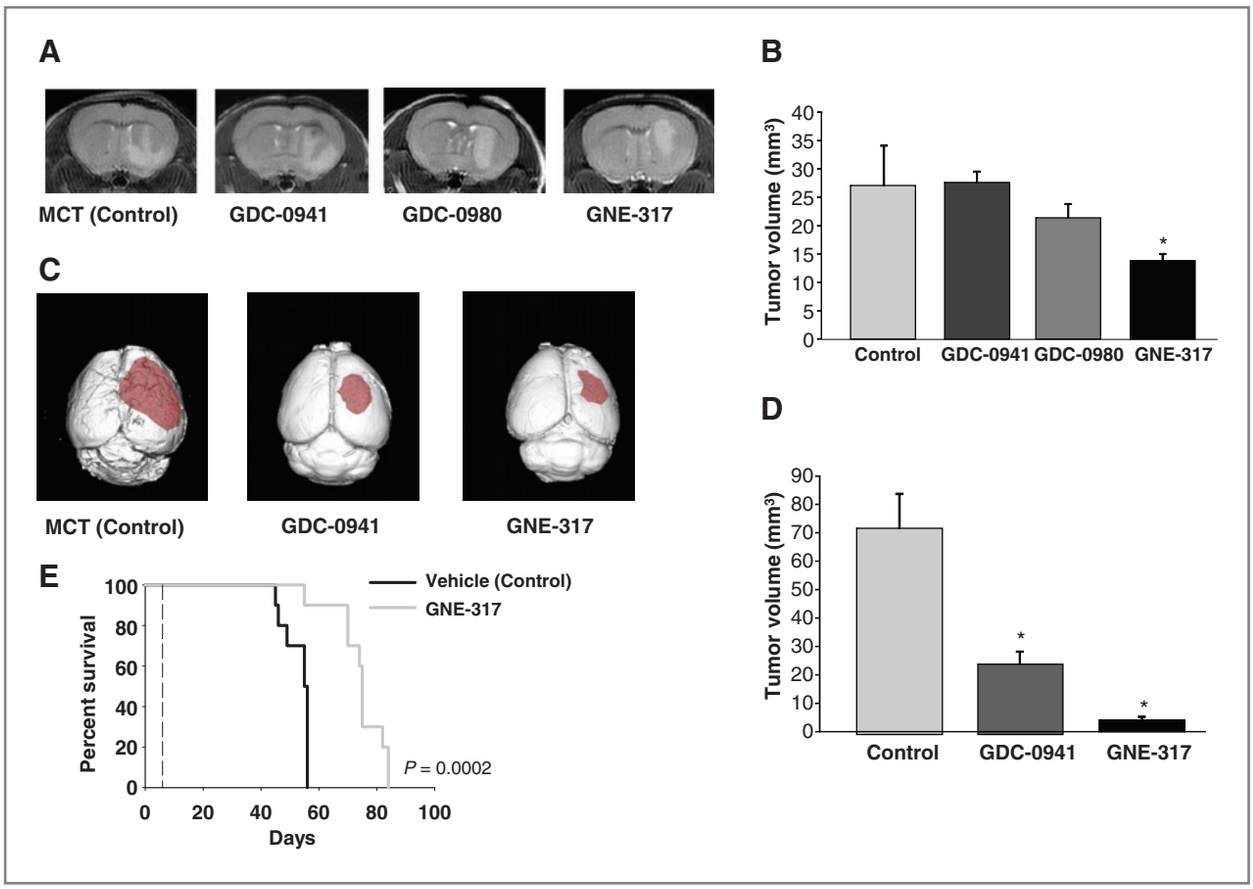

Figure 2. Efficacy in orthotopic models of glioblastoma. A, efficacy of GNE-317, GDC-0941, and GDC-0980 in GS2 neurosphere tumor model following treatment with GNE-317 at 40 mg/kg, GDC-0941 at 250 mg/kg or GDC-0980 at 10 mg/kg, daily for 6 weeks. Representative T2-weighted MRI images of brain from control and treated mice. B, GS2 brain tumor volume in control mice and mice treated with GNE-317, GDC-0941, or GDC-0980 for 6 weeks. Results are presented as the mean ± S.E. of 10 animals. C, efficacy of GNE-317 and GDC-0941 in U87 glioblastoma tumor model following treatment with GNE-317 at 40 mg/kg or GDC-0941 at 250 mg/kg, daily for 3 weeks. Representative micro-CT images of brain from control and treated mice. D, U87 brain tumor volume in control mice and mice treated with GNE-317 or GDC-0941 for 3 weeks. Results are presented as the mean ± S.E. of 10 animals. E, efficacy of GNE-317 in orthotopic GBM10 model. Survival curve for mice treated with GNE-317 PO, daily at 30 mg/kg (40 mg/kg first 2 weeks). *, $P < 0.05$ (vs. control).

90%, when compared with the vehicle control (Fig. 2D). Bioluminescence measured before and at the end of treatment (Supplementary Table 1) displayed halted tumor growth with GNE-317, which was consistent with *in vitro* findings that showed cytostasis (Supplementary Fig. 2) but no cell death. Similarly, the GS2 tumors measured by MRI (Fig. 2A) in the treated mice were more than 50% smaller than those in the control group (Fig. 2B). GDC-0941, a PI3K inhibitor that does not cross the BBB (16), was also tested in these 2 models. In contrast to GNE-317, GDC-0941 showed no activity in the GS2 model (Fig. 2A and B), whereas it was able to reduce the U87 tumor volumes by 66% (Fig. 2C and D). To assess whether the absence of efficacy of GDC-0941 was related to its lack of mTOR inhibition, the dual PI3K/mTOR inhibitor GDC-0980 (17, 18) was also tested in the GS2 model. GDC-0980 is a substrate of P-gp and bcrp1 (19). Similarly to GDC-0941, GDC-0980 showed no activity against the GS2 model (Fig. 2A and B). Plasma and brain concentrations and brain-to-plasma ratios determined at the end of the study in the GS2 tumor-bearing mice are presented in Supplementary Table 2. For the 3 compounds, the brain concentrations and brain-to-plasma ratios were comparable in the normal part of the brain and in the tumored brain. In the GBM10 model, GNE-317 was able to extend the survival of mice from a median of 55.5 to 75 days ($P < 0.05$, log rank test; Fig. 2E) when administered at 30 mg/kg (40 mg/kg the first 2 weeks).

Inhibition of the PI3K pathway in intracranial tumors

Modulation of the PI3K pathway in the GS2 and U87 tumors was determined by IHC following a single PO dose of GNE-317 (40 mg/kg) or GDC-0941 (250 mg/kg). Tissue was probed with antibodies against pAkt. GNE-317 caused a marked reduction in staining for pAkt in the GS2 tumor (Fig. 3C) when compared with the untreated animal (Fig. 3A), and led to complete suppression of signal in the U87 tumor (Fig. 3F). In contrast, GDC-0941 treatment did not cause a noticeable change of pAkt staining in GS2 tumor when compared with control (Fig. 3A and B, respectively) whereas it led to a reduction in

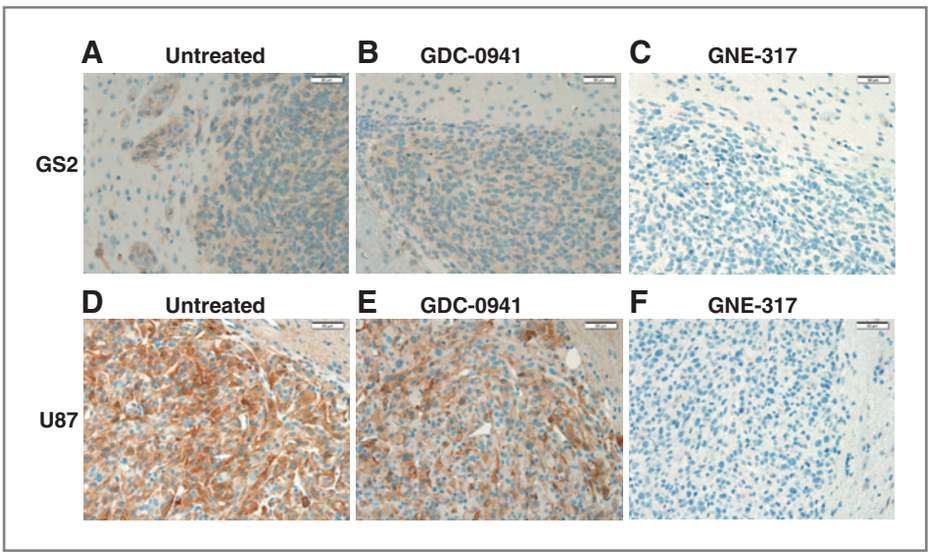

Figure 3. Immunohistochemical analysis of GS2 (A to C) and U87 (D to F) tumor-bearing brain sections from untreated mice and mice dosed with GDC-0941 (250 mg/kg) or GNE-317 (40 mg/kg). Sections were probed for the PI3K pathway marker pAkt. A and D, tumors from untreated animals; B and D, tumors from animal treated with GDC-0941; C and F, tumors from animals treated with GNE-317.

intensity and density of pAkt staining in the U87 tumor (Fig. 3D and E).

Permeability of the tumor vasculature

The integrity of the BBB in the U87 and GS2 models was assessed by DCE-MRI. The T2-weighted images show the GS2 (Fig. 4A) and U87 (Fig. 4D) intracranial tumors. In the GS2 tumors, no contrast enhancement was detected following gadolinium injection in the T1-weighted images (Fig. 4B, precontrast; and Fig. 4C, postcontrast), indicating that the BBB was intact in this tumor model. Contrary to the GS2 model, marked contrast enhancement was observed in the U87 tumors (Fig. 4E and F), confirming the presence of an impaired BBB.

Discussion

The PI3K-Akt pathway is one of the most frequently altered signaling pathways in tumors (20). In addition, activating mutations of the p110α subunit, loss of the phosphatase PTEN or activation/amplification of upstream receptor tyrosine kinases are observed in more than 80% of GBM (5), the most common malignant primary brain tumor in adults. Increased pathway signaling is also

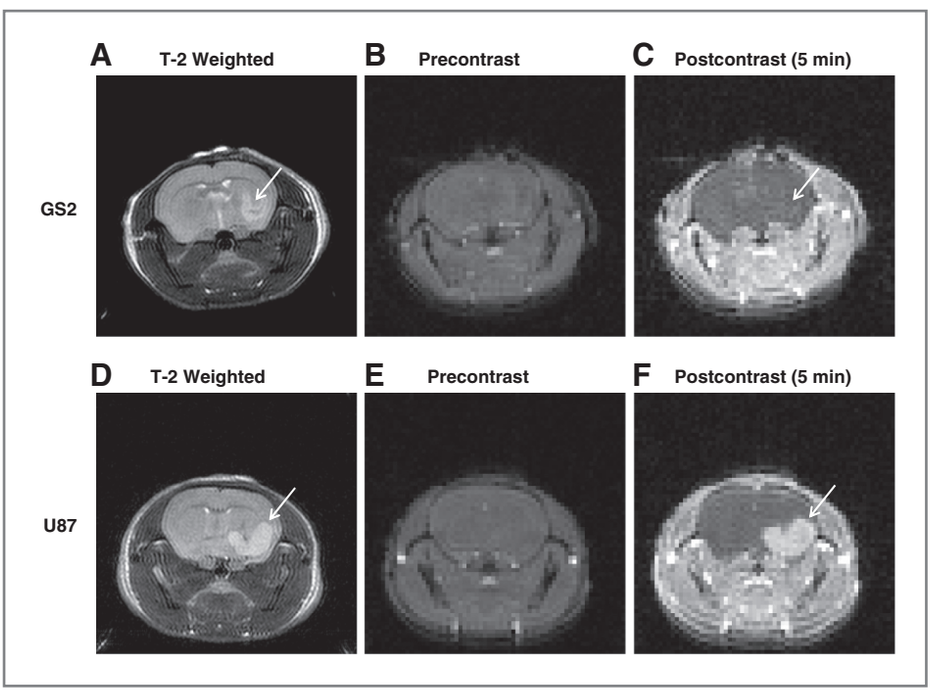

Figure 4. T2-weighted and dynamic contrast-enhanced MR imaging of GS2 and U87 intracranial tumors. A and D, T-2 weighted image of GS2 and U87 tumors, respectively. B and E, precontrast images of GS2 and U87 tumors, respectively. C and F, postcontrast images of GS2 and U87 tumors, respectively, 5 minutes following gadolinium injection. Images (C) shows no contrast enhancement in the GS2 tumors, indicating that the BBB is intact, whereas image (F) clearly shows intense contrast in the U87 tumor, confirming the disruption of the BBB in this model. Arrows point to the tumor in (A), (C), (D), and (F).

detected in response to current GBM treatments, such as radiation and chemotherapy (21, 22). Inhibiting this pathway in the brain remains challenging however, as compounds have to cross the BBB to reach their target. Although the BBB may be disrupted in most brain tumors (23), which allows some exposure to the compounds, spreading edges of neoplasms are frequently shielded by an intact BBB and the protective function of efflux transporters expressed in the endothelial cells of the brain capillaries (24). Thus, effective treatment of primary brain tumors or brain metastases can only be achieved with molecules that are able to cross the BBB. GNE-317 (Fig. 1A) was designed to bypass the 2 main transporters constituting the BBB, P-gp and BCRP.

To that end, we found that for the thienopyrimidine series of PI3K/mTOR inhibitors, the CNS-MPO score, an algorithm which assigns a numerical value to a balance of 6 distinct physicochemical properties (10), correlated with the likelihood of P-gp or bcrp1-mediated efflux. In an evaluation of more than 20 thienopyrimidines, a CNS-MPO score of less than 4.5 increased the probability that the compound would be substrate of both P-gp and bcrp1 (Supplementary Fig. 1). Therefore, newly designed compounds were evaluated *in silico* before synthesis to ensure that the CNS-MPO score was greater than 4.5 (for additional discussion, see Heffron and colleagues, manuscript in preparation). Of the compounds designed according to the CNS-MPO guidelines, GNE-317, a selective (Supplementary Table 3) inhibitor of PI3K (p110α K_i 5 nM) and mTOR (K_i 11 nM), with EC_{50} for growth inhibition of glioma cell lines ranging from 0.16 to 1.17 μmol/L (Supplementary Table 4), was further evaluated. This compound showed inhibition greater than 50% for 6 of the 59 kinases included in the panel when tested at 1 μmol/L (all free compound). Although this was not specifically investigated in our studies, it is unlikely that meaningful inhibition of these kinases occurred *in vivo* as the highest GNE-317 free brain concentration would not exceed 0.4 μmol/L (based on plasma and brain binding and data presented in Fig. 1B).

Studies in MDCK and LLC-PK cells overexpressing human or mouse P-gp or BCRP indicated that this compound was not a good substrate of these transporters (Table 1). These *in vitro* results suggesting that GNE-317 brain penetration would not be markedly hindered were consistent with the data obtained *in vivo*. In mice, free brain concentrations achieved after a single 50 mg/kg oral dose were greater than the pAkt IC_{50} estimated in PC3 cells (0.034 μmol/L; Heffron and colleagues, manuscript in preparation) and led to strong pathway suppression for up to 6 hours postdose (Fig. 1B–D). It is worth noting that the brain-to-plasma ratio of unbound concentration was approximately 0.3 (Table 2) and similar at 1 and 6 hours postdose. This suggested that by 1 hour, a steady-state condition had been reached between brain and plasma and that the disappearance of GNE-317 from the brain paralleled its disappearance from plasma (Fig. 1B). For drug passively permeating the BBB, the equilibrium theory of free drug applies (25), and the ratio of unbound concentrations in the brain and plasma ($C_{u,\,br}/C_{u,\,p}$) is expected to equal (or approach) 1. For GNE-317, efflux at the BBB by transporters other than P-gp and Bcrp1 may explain the lower $C_{u,\,br}/C_{u,\,p}$; experimental variability in the estimation of the free fraction in brain or plasma could also contribute to the calculation of this lower than expected free brain-to-plasma ratio. The *in vitro* determination of binding to brain homogenate has nevertheless been proposed as a reliable method to estimate free brain concentration (26). Despite this uncertainty on potential mechanisms still affecting its brain penetration, GNE-317 ability to cross the BBB constituted a remarkable improvement when compared with GDC-0941 and GDC-0980, PI3K, and PI3K/mTOR inhibitors, respectively (17, 18, 27), substrates of both P-gp and Bcrp1, which did not cause any PI3K pathway modulation in intact brain (16, 19).

Numerous small molecule inhibitors targeting components of the PI3K signaling pathway (EGFR, PI3K, AKT, and mTOR) are being evaluated in GBM patients (28). However, most of them have been showed to be substrates of Pgp and/or BCRP (29–34), and are likely to exert their effects only in areas where the BBB or blood–tumor barrier is permeable, as described by Taskar and colleagues with lapatinib (35).

The marked inhibition of the PI3K pathway in the brain of mice with intact BBB (Fig. 1C), evidenced by the significant suppression of the PI3K and mTOR markers pAkt, p4EBP1, and pS6, suggested that GNE-317 could be efficacious in intracranial tumors driven by activation of this pathway. Studies in the U87 and GS2 orthotopic models of GBM showed that GNE-317 could reduce tumor volumes by 90% and 50%, respectively (Fig. 2). The U87 cells were selected as a well characterized and widely used glioma model (36, 37). However, in contrast to human GBM, this model presents an impaired BBB by DCE- MRI (Fig. 4E and F and ref. 38), which allows even poorly brain-penetrant compounds to reach the tumor. Thus, this model represents what might occur in contrast-enhancing region(s) of a brain tumor. Consistent with these findings, GDC-0941 was efficacious in this orthotopic model and able to reduce the tumor volume by more than 60% (Fig. 2C and D) despite very poor brain penetration in the presence of an intact BBB (16). Tumor penetration has also been observed with topotecan, (a substrate of P-gp and BCRP), which achieved a significantly higher unbound concentration in the U87 tumor than in the healthy contralateral brain (38). Hence, the effect observed with GNE-317, although promising and consistent with PI3K inhibition, was not unexpected and did not fully illustrate the greater potential of brain-penetrant compounds for the treatment of brain tumors. In contrast, the GS2 model presents an intact BBB (Fig. 4B and C) and recapitulates the invasiveness of GBM. GNE-317 was efficacious in that model whereas no activity was observed with GDC-0941 or GDC-0980 (Fig. 2A and B). The marked contrast in the efficacy of GDC-0941 in the U87 model versus complete lack of effect in the GS2 model further emphasizes the importance of brain penetration for optimal effect. For each compound, the concentrations were similar in the normal part of the brain and the tumored

brain (Supplementary Table 2). This was consistent with the presence of an unaltered BBB; indeed, if the BBB in the GS2 model were disrupted, GDC-0941 and GDC-0980 concentrations would most likely be higher in the tumor-bearing side than in the normal brain, as reported for topotecan in the U87 model (38). In the GBM10 model, mice that were treated with GNE-317 experienced a marked survival benefit (Fig. 2E), indicating that GNE-317 was also efficacious in an *in vivo*-passaged xenograft model that had not been exposed to tissue culture conditions.

PI3K pathway suppression in the intracranial tumors, assessed by IHC, was consistent with the efficacy and BBB findings. GDC-0941, unable to cross an intact BBB, did not cause a noticeable change in pAkt staining in the GS2 tumor when compared with control, whereas the suppression of the pathway was marked following treatment with GNE-317 (Fig. 3A and C). In the U87 tumor, GDC-0941 did reduce the density and intensity of the pAkt staining (Fig. 3E) when compared with control (Fig. 3D), in agreement with its ability to cross the disrupted BBB of this tumor, whereas GNE-317 treatment led to the complete suppression of pAkt staining (Fig. 3F).

For all compounds tested, the brain-to-plasma ratios determined in the GS2 tumor-bearing mice at the end of study (Supplementary Table 2) were consistent with those obtained in CD-1 mice (Table 2) with GNE-317 after a single dose and, for GDC-0941, values were similar to what was previously described (16). The greater concentrations reached throughout the brain with GNE-317, when compared with GDC-0941 and GDC-0980, underscored the importance of efficient brain penetration to achieve efficacy in the presence of an intact BBB. These results clearly showed that although some compounds may be active in areas of brain tumors (primary or metastases) that have disrupted BBB and capture contrast agents, efficient antitumor activity on invasive areas with intact BBB requires compounds able to cross the BBB, such as GNE-317.

This report is, to our knowledge, the first describing the properties and efficacy of a PI3K inhibitor specifically designed to cross the BBB, with the treatment of GBM and possibly other PI3K-dependent CNS tumors as the primary objective. Although inhibition of PI3K may be associated with adverse effects, including ones related to the role of this pathway in glucose metabolism, this compound and potentially others optimized with the same purpose may provide a much needed treatment option for GBM. In addition, such brain-penetrant compounds, more likely to reach their target, should allow a more reliable assessment of biologic and pharmacodynamic hypotheses.

Disclosure of Potential Conflicts of Interest

J.N. Sarkaria is the recipient of a grant from Genentech, Inc. J.L. Pokorny reported no conflict of interest. No potential conflicts of interest were disclosed by other authors.

Authors' Contributions

Conception and design: L. Salphati, T.P. Heffron, R.A. Carano
Development of methodology: L. Salphati, R.A. Carano, J. Greve
Acquisition of data (provided animals, acquired and managed patients, provided facilities, etc.): B. Alicke, M. Nishimura, K. Barck, J. Cheong, J. Greve, S. Kharbanda
Analysis and interpretation of data (e.g., statistical analysis, biostatistics, computational analysis): L. Salphati, T.P. Heffron, K. Barck, R.A. Carano, J. Cheong, J. Greve
Writing, review, and/or revision of the manuscript: L. Salphati, T.P. Heffron, B. Alicke, K. Barck, R.A. Carano, J. Cheong
Administrative, technical, or material support (i.e., reporting or organizing data, constructing databases): L. Salphati, J. Cheong, K.A. Edgar
Study supervision: R.A. Carano

The costs of publication of this article were defrayed in part by the payment of page charges. This article must therefore be hereby marked *advertisement* in accordance with 18 U.S.C. Section 1734 solely to indicate this fact.

Received March 1, 2012; revised August 8, 2012; accepted August 27, 2012; published OnlineFirst September 19, 2012.

References

1. Engelman JA, Luo J, Cantley LC. The evolution of phosphatidylinositol 3-kinases as regulators of growth and metabolism. Nat Rev Genet 2006;7:606–19.
2. Engelman JA. Targeting PI3K signalling in cancer: opportunities, challenges and limitations. Nat Rev Cancer 2009;9:550–62.
3. Luo J, Manning BD, Cantley LC. Targeting the PI3K-Akt pathway in human cancer: rationale and promise. Cancer Cell 2003;4:257–62.
4. Akhavan D, Cloughesy TF, Mischel PS. mTOR signaling in glioblastoma: lessons learned from bench to bedside. Neuro Oncol 2010;12:882–9.
5. Network TCGAR. Comprehensive genomic characterization defines human glioblastoma genes and core pathways. Nature 2008;455:1061–8.
6. Lino MM, Merlo A. PI3Kinase signaling in glioblastoma. J Neurooncol 2011;103:417–27.
7. Adamson C, Kanu OO, Mehta AI, Di C, Lin N, Mattox AK, et al. Glioblastoma multiforme: a review of where we have been and where we are going. Expert Opin Investig Drugs 2009;18:1061–83.
8. Mellinghoff IK, Schultz N, Mischel PS, Cloughesy TF. Will Kinase Inhibitors Make it as Glioblastoma Drugs? Curr Top Microbiol Immunol 2011.
9. Tanaka K, Babic I, Nathanson D, Akhavan D, Guo D, Gini B, et al. Oncogenic EGFR signaling activates an mTORC2-NF-kappaB pathway that promotes chemotherapy resistance. Cancer Discov 2011;1:524–38.
10. Wager TT, Hou X, Verhoest PR, Villalobos A. Moving beyond rules: the development of a central nervous system multiparameter optimization (CNS MPO) approach to enable alignment of druglike properties. ACS Chem Neurosci 2010;1:435–49.
11. Kalvass JC, Maurer TS, Pollack GM. Use of plasma and brain unbound fractions to assess the extent of brain distribution of 34 drugs: comparison of unbound concentration ratios to *in vivo* p-glycoprotein efflux ratios. Drug Metab Dispos 2007;35:660–6.
12. Gunther HS, Schmidt NO, Phillips HS, Kemming D, Kharbanda S, Soriano R, et al. Glioblastoma-derived stem cell-enriched cultures form distinct subgroups according to molecular and phenotypic criteria. Oncogene 2008;27:2897–909.
13. Carlson BL, Pokorny JL, Schroeder MA, Sarkaria JN. Establishment, maintenance and *in vitro* and *in vivo* applications of primary human glioblastoma multiforme (GBM) xenograft models for translational biology studies and drug discovery. Curr Protoc Pharmacol. 2011;52:1–14.

14. Chen R, Nishimura MC, Bumbaca SM, Kharbanda S, Forrest WF, Kasman IM, et al. A hierarchy of self-renewing tumor-initiating cell types in glioblastoma. Cancer Cell 2010;17:362–75.
15. de Crespigny A, Bou-Reslan H, Nishimura MC, Phillips H, Carano RA, D'Arceuil HE. 3D micro-CT imaging of the postmortem brain. J Neurosci Methods 2008;171:207–13.
16. Salphati L, Lee LB, Pang J, Plise EG, Zhang X. Role of P-glycoprotein and breast cancer resistance protein-1 in the brain penetration and brain pharmacodynamic activity of the novel phosphatidylinositol 3-kinase inhibitor GDC-0941. Drug Metab Dispos 2010;38:1422–6.
17. Sutherlin DP, Bao L, Berry M, Castanedo G, Chuckowree I, Dotson J, et al. Discovery of a potent, selective, and orally available class I phosphatidylinositol 3-kinase (PI3K)/mammalian target of rapamycin (mTOR) kinase inhibitor (GDC-0980) for the treatment of cancer. J Med Chem 2011;54:7579–87.
18. Wallin JJ, Edgar KA, Guan J, Berry M, Prior WW, Lee L, et al. GDC-0980 is a novel class I PI3K/mTOR kinase inhibitor with robust activity in cancer models driven by the PI3K pathway. Mol Cancer Ther 2011; 10:2426–36.
19. Pang J, Baumgardner M, Ding X, Edgar KA, Plise EG, Wallin JJ, et al. Preclinical evaluation of a novel PI3K/mTor inhibitor and prediction of its human pharmacokinetics. Drug Metabol Rev 2009;41:164 (Abstract 332).
20. Liu P, Cheng H, Roberts TM, Zhao JJ. Targeting the phosphoinositide 3-kinase pathway in cancer. Nat Rev Drug Discov 2009;8:627–44.
21. Keunen O, Johansson M, Oudin A, Sanzey M, Rahim SA, Fack F, et al. Anti-VEGF treatment reduces blood supply and increases tumor cell invasion in glioblastoma. Proc Natl Acad Sci U S A 2011;108:3749–54.
22. Li HF, Kim JS, Waldman T. Radiation-induced Akt activation modulates radioresistance in human glioblastoma cells. Radiat Oncol (London, England) 2009;4:43.
23. Huse JT, Holland EC. Targeting brain cancer: advances in the molecular pathology of malignant glioma and medulloblastoma. Nat Rev Cancer 2010;10:319–31.
24. de Vries NA, Beijnen JH, Boogerd W, van Tellingen O. Blood-brain barrier and chemotherapeutic treatment of brain tumors. Expert Rev Neurother 2006;6:1199–209.
25. Tillement JP, Urien S, Chaumet-Riffaud P, Riant P, Bree F, Morin D, et al. Blood binding and tissue uptake of drugs. Recent advances and perspectives. Fundam Clin Pharmacol 1988;2:223–38.
26. Liu X, Van Natta K, Yeo H, Vilenski O, Weller PE, Worboys PD, et al. Unbound drug concentration in brain homogenate and cerebral spinal fluid at steady state as a surrogate for unbound concentration in brain interstitial fluid. Drug Metab Dispos 2009;37:787–93.
27. Folkes AJ, Ahmadi K, Alderton WK, Alix S, Baker SJ, Box G, et al. The identification of 2-(1H-indazol-4-yl)-6-(4-methanesulfonyl-piperazin-1-ylmethyl)-4-morpholin-4-yl-t hieno[3,2-d]pyrimidine (GDC-0941) as a potent, selective, orally bioavailable inhibitor of class I PI3 kinase for the treatment of cancer. J Med Chem 2008;51:5522–32.
28. Holand K, Salm F, Arcaro A. The phosphoinositide 3-kinase signaling pathway as a therapeutic target in grade IV brain tumors. Curr Cancer Drug Targets 2011;11:894–918.
29. de Vries NA, Buckle T, Zhao J, Beijnen JH, Schellens JH, van Tellingen O. Restricted brain penetration of the tyrosine kinase inhibitor erlotinib due to the drug transporters P-gp and BCRP. Invest New Drugs 2012;30:443–9.
30. Lagas JS, van Waterschoot RA, Sparidans RW, Wagenaar E, Beijnen JH, Schinkel AH. Breast cancer resistance protein and P-glycoprotein limit sorafenib brain accumulation. Mol Cancer Ther 2010;9:319–26.
31. Poller B, Wagenaar E, Tang SC, Schinkel AH. Double-transduced MDCKII cells to study human P-glycoprotein (ABCB1) and breast cancer resistance protein (ABCG2) interplay in drug transport across the blood-brain barrier. Mol Pharm 2011;8:571–82.
32. Polli JW, Humphreys JE, Harmon KA, Castellino S, O'Mara MJ, Olson KL, et al. The role of efflux and uptake transporters in [N-{3-chloro-4-[(3-fluorobenzyl)oxy]phenyl}-6-[5-({[2-(methylsulfonyl)ethyl]amino} methyl)-2-furyl]-4-quinazolinamine (GW572016, lapatinib) disposition and drug interactions. Drug Metab Dispos 2008;36:695–701.
33. Polli JW, Olson KL, Chism JP, John-Williams LS, Yeager RL, Woodard SM, et al. An unexpected synergist role of P-glycoprotein and breast cancer resistance protein on the central nervous system penetration of the tyrosine kinase inhibitor lapatinib (N-{3-chloro-4-[(3-fluorobenzyl) oxy]phenyl}-6-[5-({[2-(methylsulfonyl)ethyl]amino}methyl)-2-furyl]-4-quinazolinamine; GW572016). Drug Metab Dispos 2009;37:439–42.
34. Tang SC, Lagas JS, Lankheet NA, Poller B, Hillebrand MJ, Rosing H, et al. Brain accumulation of sunitinib is restricted by P-glycoprotein (ABCB1) and breast cancer resistance protein (ABCG2) and can be enhanced by oral elacridar and sunitinib coadministration. Int J Cancer 2012;130:223–33.
35. Taskar KS, Rudraraju V, Mittapalli RK, Samala R, Thorsheim HR, Lockman J, et al. Lapatinib distribution in HER2 overexpressing experimental brain metastases of breast cancer. Pharm Res 2012; 29:770–81.
36. Clark MJ, Homer N, O'Connor BD, Chen Z, Eskin A, Lee H, et al. U87MG decoded: the genomic sequence of a cytogenetically aberrant human cancer cell line. PLoS Genet 2010;6:e1000832.
37. Weller M, Rieger J, Grimmel C, Van Meir EG, De Tribolet N, Krajewski S, et al. Predicting chemoresistance in human malignant glioma cells: the role of molecular genetic analyses. Int J Cancer 1998;79:640–4.
38. Carcaboso AM, Elmeliegy MA, Shen J, Juel SJ, Zhang ZM, Calabrese C, et al. Tyrosine kinase inhibitor gefitinib enhances topotecan penetration of gliomas. Cancer Res 2010;70:4499–508.